Quantum Cascade Laser Subject to Filtered-phase-Conjugate Feedback: Stability, Root Locus Analysis, and Particle Swarm Optimization

Fahimeh Bakhsheshi[a], Khosro Mabhouti[a,*], Rahim Naderaliand[a], and Ali Mahmoudloo[b]

[a]Department of Physics, Faculty of Sciences, Urmia University, Urmia, Iran
[b]Department of Physics Education, Farhangian University, Tehran, Iran

[*]Corresponding author email: kh.mabhouti@urmia.ac.ir

Regular paper: Received: Jul.07, 2024, Revised: Mar. 29, 2025 Accepted: July 10, 2025, Available Online: July 12, 2025
DOI: 10.61186/ijop.18.1.19

ABSTRACT— Quantum cascade lasers (QCLs) are sources in mid-infrared and terahertz (THz) regions used in the sensing domain and quality control. This paper investigates QCLs subject to filtered phase-conjugate feedback (FPCF). Instabilities can be detected using the graphical method of pole analysis and the particle swarm optimization algorithm, which allows us to identify and characterize the limitation and critical relations between the laser operating parameters. There is good agreement between the two methods to stability boundaries. The effects of FPCF in comparison with conventional optical feedback (COF), phase-conjugate feedback (PCF), and tilted optical feedback (TOF) show that the penetration time factor has a significant and greater influence on the stability of QCL subject to FPCF. These results are in perfect agreement with previous experimental and analytical studies.

KEYWORDS: Quantum cascade laser, stability, Pole analysis, PSO algorithm.

I. INTRODUCTION

Optical feedback is a powerful and effective way to modify and trigger semiconductor lasers (SLs) to generate rich nonlinear dynamics [1]–[3]. In most laser configurations, the feedback occurs to different extents, making it necessary to include it in the operational models of many laser systems. Optical feedback strongly affects laser performance. Depending on the feedback strength, Line width narrowing and broadening, threshold change, mode-hopping, and intensity-noise degradation have been observed [4], [5]. There are different types of feedback, such as conventional optical feedback (COF) [6],[7], phase-conjugate optical feedback (PCF) [8], [9], filtered phase-conjugate optical feedback (FPCF) [10], and also tilted optical feedback (TOF) [11]. At different levels of external optical feedback, the laser output shows interesting dynamical behaviors such as a stable state, periodic and quasi-periodic oscillations, and chaos for the variations of the system parameters [6]. The main applications that can be mentioned are related to communication purposes, optics-based information security, and displacement sensors or terahertz imaging [7], [12]. Moreover, there are several types of lasers exist, such as semiconductor lasers [6], solid-state lasers, and fiber lasers [1], [13], which, depending on the type of laser, the sensitivity to optical feedback which is related to the light reflected in the laser cavity of an external target is different [6], [14]. Quantum cascade lasers (QCLs) are another example of recently developed lasers and show interesting dynamics [6]. QCLs are tunable laser sources that have improved in performance in terms of output power and tenability [15], [16]. Versus other semiconductor lasers (SLs), QCLs are defined by picosecond carrier lifetime and exhibit a small linewidth enhancement factor (LEF) [8], [17]. QCLs are selected for applications such as aerospace countermeasures [18], sensing of environmental and chemical gases [19], lidar systems [20], and open space communications

[Downloaded from mail.ijop.ir on 2026-11-26]

[21]. Recently, the stability analysis of QCLs subject to COF, PCF [7], [8], and also tilted optical feedback (TOF) [11], [22] has been studied. QCLs under COF exhibit stable behavior [2], which is why that isn't easy to generate pulse oscillations in QCLs through COF [11]. When a QCL is considered subject to PCF, it has illustrated a considerable variety in the dynamics; hence it can be said that PCF destabilizes the QCL [8], [10]. On the other hand, the QCL can become unstable under tilted-angle optical feedback, while it exhibits stability under common optical feedback [2], [21]. As the tilted feedback angle increases, the QCL shows periodic oscillations, quasi-periodic, and low-frequency oscillations [2], [11], respectively. Considering the importance of the QCLs application as well as obtained results for COF, PCF, and TOF, it is necessary to discuss the effect of FPCF by analytical and experimental methods. In a further explanation about FPCF, it can be said a phase-conjugate mirror tends to have a peaked frequency response, a finite interaction depth, and may respond sluggishly. A finite interaction depth or slow response conjugate phase feedback is considered in semiconductor lasers. The penetration time τ_r of light into the conjugate phase medium is a significant parameter of finite response conjugate phase feedback. Compared to PCF, it was observed that the stability increases slightly with increasing τ_r, which is due to the spectral filtering caused by the reflected field mirror that suppresses frequencies larger than $\frac{1}{\tau_r}$ [23], [24].

In this article, a QCL subject to FPCF is studied analytically. We show that QCLs subject to FPCF can become unstable. As a consequence, different nonlinear dynamics are generated, also we believe that this research work can be practical in the community of QCLs interested in the dynamical properties of these lasers. It can show a general picture of the laser performance in terms of stability and the role of different parameters in this laser. For the purpose of theoretical investigation of QCL dynamics, a three-level rate equations model is considered [10], [25]. Using certain assumptions and approximations, the rate equations for a QCL reduce to the modified Lang-Kobayashi rate equations [8]. The condition of a Hopf bifurcation is analyzed, which destabilizes the system [6], [8]. Bifurcation is a qualitative change in a system's dynamic behavior caused by variations in a parameter. A bifurcation diagram provides insight into the transition between various motion types as a system parameter changes, enabling the analysis of the system's behavior over a wide range of a key control parameter [26], [27]. In previous studies [8], [10], it is not possible to determine the asymptotic expression for the Hopf condition for higher degrees equations through approximate methods. So, for analyzing the obtained results from the higher-order characteristic equation of systems, the pole analysis technique [28], [29] and the particle swarm optimization (PSO) can be used [30], [31]. The diagram obtained from the pole analysis technique and the PSO algorithm helps to detect instabilities [32], [33]. Therefore, by using the proposed method, the characteristic equation converts to the characteristic equation of a closed-loop system [33]. Finally, the critical relations for the responses of the characteristic equation are determined by using the pole analysis and PSO algorithm.

and approximations, the rate equations for a QCL reduce to the modified Lang-Kobayashi rate equations [8]. The condition of a Hopf bifurcation is analyzed, which destabilizes the system [6], [8]. Bifurcation is a qualitative change in a system's dynamic behavior caused by variations in a parameter. A bifurcation diagram provides insight into the transition between various motion types as a system parameter changes, enabling the analysis of the system's behavior over a wide range of a key control parameter [26], [27]. In previous studies [8], [10], it is not possible to determine the asymptotic expression for the Hopf condition for higher degrees equations through approximate methods. So, for analyzing the obtained results from the higher-order characteristic equation of systems, the pole analysis technique [28], [29] and the particle swarm optimization (PSO) can be used [30], [31]. The diagram obtained from the pole analysis technique and the PSO algorithm helps

[Downloaded from mail.ijop.ir on 2026-11-26]

to detect instabilities [32], [33]. Therefore, by using the proposed method, the characteristic equation converts to the characteristic equation of a closed-loop system [33]. Finally, the critical relations for the responses of the characteristic equation are determined by using the pole analysis and PSO algorithm.

II. NUMERICAL MODEL AND STEADY STATE ANALYSIS

Quantum Cascade Laser structures, which are nanodevices, have become popular among scientific teams around the world. In quantum cascade lasers, there is a cascading structure that causes each electron to cascade through multiple active regions and generate a photon each time. Indeed, the transition of the laser happens in a region with multi-quantum wells that is a 3-level laser. A QCL usually consists of 20 to 40 periods, and electrons are transferred from one active region to the other by the tunneling effect [34]–[36]. In this paper the Long-Kobayashi equations used as numerical model that, rewritten for QCLs subject to the FPCF. This model also accords mathematically as a semiconductor laser subject to FPCF. The dimensionless rate equations are as follows [7], [10]:

$$\frac{dY}{ds}=\frac{1}{2}(1+i\alpha)(N-1)Y+\eta F \tag{1}$$

$$\frac{dF}{ds}=\frac{1}{\tau_r}\left[Y^*(s-\tau)-F\right] \tag{2}$$

$$\frac{dN}{ds}=\gamma\left[I-N\left(1+|Y|^2\right)\right] \tag{3}$$

where $Y(t)$, $F(t)$, and $N(t)$ indicate the electric field, complex feedback field and carrier population [7], [10] , respectively. The linewidth enhancement factor (LEF) α is a key parameter influencing the device's dynamic properties. LEFs ranging corresponding to QCL can be between 0.8 to 3 [8], [37]. s represents the dimensionless time [17], and η is the feedback strength, which can be seen in Eq. (1). In Eq. (2), the penetration-time and round trip time are denoted by τ_r and τ respectively [37],[10]. The ratios of the photon to carrier lifetimes in Eq. (3) are represented γ (which is given by $\gamma \equiv 2\gamma_1 A$), and the current is defined by I (where $I \equiv (P/A)+1$) [17]. If τ_r is considered zero, Eqs. (1)-(3) simplifies the equations of a PCM with zero-penetration depth [8]. According to [7], A ranges from 0.6 to 1.1. In continue, for steady states analysis of Eqs. (1)-(3), $Y = R_1 \exp(i\varphi_1)$ and $F = R_2 \exp(i\varphi_2)$ are introduced. By applying these values to Eqs. (1)-(3), the following equations are obtained:

$$\frac{dR_1}{ds}=\frac{1}{2}(N-1)R_1+\eta R_2\cos(\varphi_2-\varphi_1) \tag{4}$$

$$\frac{d\varphi_1}{ds}=\frac{\alpha}{2}(N-1)+\eta\frac{R_2}{R_1}\sin(\varphi_2-\varphi_1) \tag{5}$$

$$\frac{dN}{ds}=\gamma\left[I-N\left(1+R_1^2\right)\right] \tag{6}$$

$$\frac{dR_2}{ds}=\frac{1}{\tau_r}\left\{R_1(s-\tau)\cos[\varphi_1(s-\tau)+\varphi_2]-R_2\right\} \tag{7}$$

$$\frac{d\varphi_2}{ds}=-\frac{1}{\tau_r}\left\{\frac{R_1(s-\tau)}{R_2}\sin(\varphi_1(s-\tau)+\varphi_2)\right\} \tag{8}$$

The steady-state solutions such as PCM produce zero depth. By assuming the feedback strength η as a control parameter [7] and the conditions of Eqs. (4)-(8) equal to zero, the steady-state solutions are calculated:

$$R_1^2=\frac{I-N}{N} \tag{9}$$

$$N=\pm\frac{2\eta}{\sqrt{1+\alpha^2}}+1 \tag{10}$$

Now, the linear stability of equations (4)-(8) can be performed. Therefore, the eigenvalues of the linear variable equation must be considered [17]:

$$M\equiv\lambda-B_1-B_2\,e^{-S\lambda} \tag{11}$$

[Downloaded from mail.ijop.ir on 2026-11-26]

From the linearized equations and with the assumption $C=\frac{1}{2}(N\text{-}1)$, the Jacobian matrix is determined, and the characteristic equations for the growth rate λ are obtained:

$$\begin{pmatrix} C & -\alpha CR & \frac{1}{2}R & -C & \alpha CR \\ \frac{\alpha C}{R} & C & \frac{\alpha}{2} & -\frac{\alpha C}{R} & -C \\ -2\gamma(2C+1) & 0 & -\gamma(1+R^2) & 0 & 0 \\ \frac{1}{\tau_r}e^{-s\lambda} & 0 & 0 & -\frac{1}{\tau_r} & 0 \\ 0 & -\frac{1}{\tau_r}e^{-s\lambda} & 0 & 0 & -\frac{1}{\tau_r} \end{pmatrix} \quad (12)$$

In order to determine Hopf conditions, $\lambda=i\sigma$ [38] is introduced. The parameter σ represents the Hopf bifurcation frequency. Due to the separation between the imaginary and real parts, we obtained two equations for σ and C:

$$\begin{aligned} &\sigma^4\left\{\tau_r\left(2(1-C\tau_r)+\gamma\tau_r\left(1+R^2\right)\right)\right\}-\sigma^2\times \\ &\times\left\{\left(1+\alpha^2\right)\left[\left[-\gamma CR^2{\tau_r}^2\left(1+C\right)+C^2{\tau_r}^2\left(\gamma+2\right)\right]+\right.\right. \\ &\left.+\gamma\left(\left(1+R^2\right)+2\tau_r R^2\right)-2C\left(2\tau_r\gamma+1\right)\right\}- \\ &-\sigma\left\{\sin\left(2\sigma\tau\right)C^2\left(1+\alpha^2\right)+\sin\left(\sigma\tau\right)\left[\gamma CR^2\tau_r+\right.\right. \\ &\left.\left.+2\gamma C^2R^2\tau_r\left(1+\alpha^2\right)\right]\right\}-C^2\gamma\cos\left(2\sigma\tau\right)\left(1+\alpha^2\right)\times \\ &\times\left(1+R^2\right)-\left(\cos\left(\sigma\tau\right)+1\right)\left[\gamma CR^2\left(1+\alpha^2\right)\right. \\ &\left.++2C^2R^2\left(1+\alpha^2\right)\right]=0 \end{aligned} \quad (13)$$

$$\begin{aligned} &-{\tau_r}^2\sigma^5-\sigma^3\left\{C\tau_r\left(C\tau_r\left(1+\alpha^2\right)-2\left(\gamma\tau_r+2\right)\right)+\right. \\ &\left.+\tau_r\left(2\gamma\left(1+R^2\right)+\tau_r R^2\right)+1\right\}-\sigma\left\{C^2\left(1+\alpha^2\right)\times\right. \\ &\left.\times\left(\cos\left(2\sigma\tau\right)-1\right)+\gamma\left(2C-R^2\right)+\left(\cos\left(\sigma\tau\right)+1\right)\times\right. \\ &\left.\times\left[\gamma CR^2\tau_r+2\gamma C^2R^2\tau_r\left(1+\alpha^2\right)\right]+\left(1+\alpha^2\right)\times\right. \\ &\left.\times\left[2C\gamma\tau_r\left(R^2-C\right)\right]\right\}+C\gamma\left(1+\alpha^2\right)\left[\sin\left(2\sigma\tau\right)\times\right. \\ &\left.\times\left(1+R^2\right)\right]+CR^2\sin\left(\sigma\tau\right)\left(1+\alpha^2\right)\left[\gamma+2C\right]=0 \end{aligned} \quad (14)$$

Along with Eqs. (13) and (14), the values of σ at a Hopf bifurcation point are presented. In the limit value of γ, the conformity of these equations is correctly verified by the conditions obtained in [10]. However, the solutions of the mentioned equations are sought in order of 1 value of γ. Recently, studies have shown that a relatively high feedback rate induces the first dynamic instabilities in QCLs [7].

III. ROUND TRIP TIME (τ) AND PENETRATION TIME (τ_r)

In this section, the influence of the round trip time τ, penetration time τ_r, pump parameter P, and the linewidth enhancement factor α on the stability boundaries of the system was studied. The results show that QCL subject to FPCF can present a series of nonlinear dynamics such as steady state, period doubling, and chaos by changing the mentioned parameters. To investigate the influences of the τ_r on laser dynamics, bifurcation diagrams were proposed in terms of the values of τ_r and η as the bifurcation parameter. Figure 1 shows the schematic of our numerical model for the QCL subject to FPCF. Moreover, η is tunable and can be defined as the bifurcation parameter. Some of the numbers used are based on previous studies [7], [10], [18]. As shown in Fig. 1(a), it seems that when the value of τ_r is small, there is a change in the laser output power. Specifically, at $\tau_r=0.5$, the laser exhibits various oscillations despite having $\alpha=3$ and $\tau=20$. Figure 1(b) shows that the dynamic variation decreases as the value of P increases, while all other parameters remain constant compared to Fig. 1(a). Figure 1(c) depicts the significant impact of changing τ_r ($\tau_r=1$) and α ($\alpha=2$) values on laser output. Specifically, increasing τ_r and decreasing α cause a noticeable shift in the dynamics of the laser output. It appears that the figure only shows the bifurcation and the onset of instability. Other features may not be visible in this context.

[Downloaded from mail.ijop.ir on 2026-11-26]

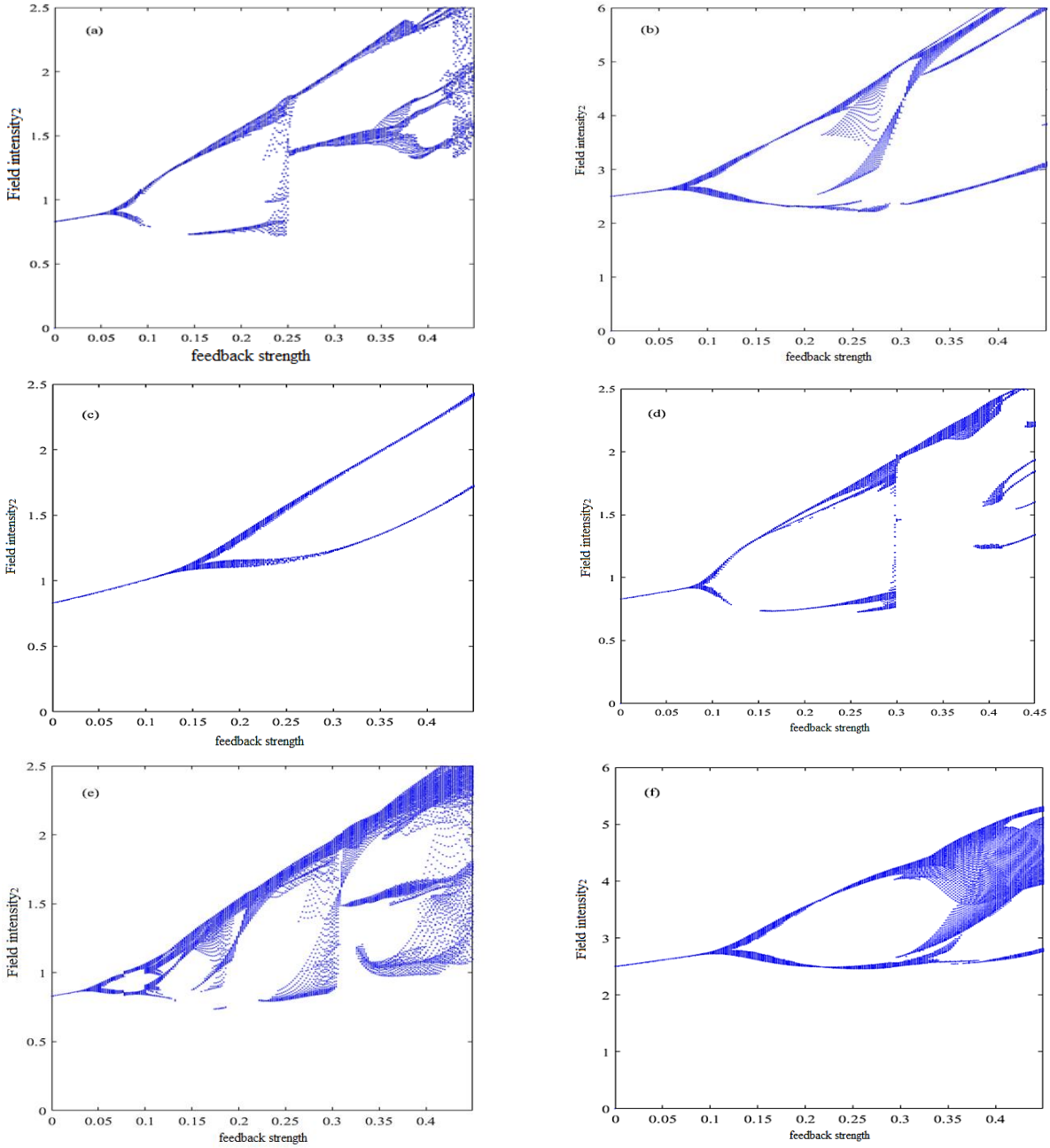

Fig. 1. Bifurcation diagrams for the extreme of the output intensity $|E|^2$ with η as the bifurcation parameter for (a) and (b) τ_r=0.5, α=3, and τ=20, (c) τ_r=1, α=2, and τ=20, (d) τ_r=1, α=3, and τ=20, (e) τ_r=1, α=3, and τ=50, (f) $\tau_r = 1$, α=3, and τ=20. The values of the parameters are fixed to P=0.5, γ=3.3, I=1.83 in Figs. 1(a) and 1(c)–1(e), and P=1.5, γ=3.3, I=3.5 in Figs. 1(b) and 1(f), respectively.

The presence of bifurcation, and other dynamics, is shown in Fig. 1(d). The dynamics have noticeable changes through the increase of LEF. Figure 1(d) provides an example of chaotic oscillations of the laser output for $\alpha = 3$, but other parameters are the same as in Fig. 1(c). In this case, through a further increment in the LEF value, the laser output demonstrates different regions, including quasi-periodic oscillations and, finally chaotic oscillations. Figure 1(e) represents the $\tau = 50$ and $\tau_r = 1$. With increasing τ, the laser output shows a more chaotic regime. As P increases from 0.5 to 1.5, the regional shape of the dynamics changes; hence bifurcation, period

[Downloaded from mail.ijop.ir on 2026-11-26]

doubling, and chaos can be observed as shown in Fig. 1(f).

In short, it can be written that the stability of the quantum cascade system, due to its sensitivity to feedback, is strongly dependent on changes in important parameters such as τ_r and α. The penetration depth time τ_r parameter increases in the system, creating more instability, and we witness more dynamics. Another significant parameter can be called α. Which increases and decreases, and QCL becomes more stable or unstable.

IV. ASYMPTOTIC ANALYSIS

A. *Asymptotic Analysis for Values of* τ_r

In this subsection, asymptotic expressions are determined for Hopf bifurcation conditions. The details of the steady-state solutions and Hopf bifurcation conditions, as discussed in the previous section. According to values of τ_r and fixed parameters, we can reduce Eqs. (13) and (14) (Eqs. (13) and (14) are in the order of ${\tau_r}^2$) as follows:

$$\sigma^2 = \left[-C^2\left(1+\alpha^2\right) + \gamma\left(2C - \frac{I-2C-1}{2C+1} \right) \right] \tag{15}$$

$$\begin{aligned} & 2C^3\left(1+\alpha^2\right) + \\ & +C^2\left[-2\left(1+\alpha^2\right)\frac{(\gamma+1)}{2C+1} + 2\left(1+\alpha^2\right) - 4\gamma \right] + \\ & +C\left\{ \frac{\gamma I}{2C+1}\left[(2\gamma+1) - \left(1+\alpha^2\right) \right] - 2\gamma \right\} - \\ & -\frac{\gamma^2 I}{2C+1}\left(\frac{I}{2C+1} - 1 \right) = 0 \end{aligned} \tag{16}$$

In the following, an expression for feedback strength η is derived from Eqs. (9) and (10):

$$\eta = |C|\sqrt{1+\alpha^2} \tag{17}$$

One can obtain an expression for pump current I as a function of critical values *C* by rewriting Eq. (16), leading to:

$$\begin{aligned} & -I^2\left(\frac{\gamma^2}{(2C+1)^2} \right) + \\ & +I\left\{ \frac{\gamma^2}{(2C+1)} + \frac{\gamma C}{(2C+1)}\left[(2\gamma+1) - \left(1+\alpha^2\right) \right] \right\} + \\ & +\left\{ +2C^3\left(1+\alpha^2\right) + C^2\left[-2\left(1+\alpha^2\right)\frac{(\gamma+1)}{(2C+1)} + \right.\right. \\ & \left.\left. +2\left(1+\alpha^2\right) - 4\gamma \right] - 2\gamma C \right\} = 0 \end{aligned} \tag{18}$$

To derive critical points from the characteristic Eq. (16), one cannot use the approximations applied in Ref. [10], as regards γ is different for the type of QCL lasers than SLs. For conventional SL, γ is typically in the order of 10^{-3} [7]; therefore, the same method used in previous studies cannot be expected to be applicable in this case. As a result, various nonlinear dynamics emerge, and we believe that this research will be valuable to the QCL community focused on the dynamical properties of these lasers. In the following, using the pole analysis method shows that critical points can be achieved for the fifth-order equation and determine which points and roots can change the nature of the system.

V. POLE ANALYSIS

For the pole analysis of Eq. (18) and the extraction of critical relations, the following equation can be obtained by using the Root-Locus (RL) method [39]. The root locus method works by plotting the movement of the closed-loop poles located in the s-plane, taking the transfer function as a gain parameter [40]. Walter R. Evans [32] invented stability in classical control system. In mathematics, Laplace transforms are graphed on a complex s-plane. In control theory, the root locus method uses a graphical plot to test the effect of variation of specific system parameters, with the variation of controller gain within a

[Downloaded from mail.ijop.ir on 2026-11-26]

feedback control system, on the system's roots [41]. Due to the use of a complex s-plane, instead of using the time domain, the frequency domain can be employed in processes [41]. It can use as a graphical analysis tool in physics and engineering [40]. As an advantage of the root locus technique, we can comment on the stability of systems without any need to write conventional techniques. The stability criterion has the advantage of reducing the order of the equations that must be handled and applies to systems with more than one variable parameter [28], [29], [42].

In this study, the RL method analyzes the poles via plotting the paths traveled by the locations of the characteristic Eq. (19) as adjustable K ranges (as gain) from 0 to $+\infty$ [39]. Thus, to make use of the RL method, Eq. (18) should be rewritten as Eq. (A3) (see Appendix A) form, and then has been written as the following equation:

$$1+\frac{K\left\{4X^5+8X^4+\left[1-2I(\gamma+1)+4\right]X^3+\left[-I(\gamma+1)+1-\gamma I\right]X^2-\frac{1}{2}\gamma IX\right\}}{-16\gamma X^4-24\gamma X^3+\left[-12\gamma+2\gamma I(2\gamma+1)\right]X^2+\left[\gamma I(2\gamma+1)-2\gamma+2\gamma^2 I\right]X-\gamma^2 I(I-1)}=0 \quad (19)$$

This equation is a transform function. The coefficients used to calculate the above relation are in Appendix (A).

Figures. 2(a) and 2(b) show the results of calculations for the transfer function, which display in a typical root-locus plot. The coefficients used to calculate the above relationship can be found in Appendix B. In these diagrams, the poles of Eq. (19) are analyzed, and each of the poles is the root of Eq. (18). According to Eq. (19), the five poles can be obtained. Each of them can change the nature of the stability of Eq. (18). The horizontal and the vertical axis show the real and the imaginary values of poles, respectively.

In this analysis, *K* tends from 0 to infinity as long as the poles can continue for the specific value of K, the nature of the poles can change, and the stability condition eliminates.

As shown in Fig. 2(a) and 2(b), all five poles change with increasing K value. However, for two defined poles in a given *K*, the system's stability changes from the real to the imaginary. It is the first Hopf point, and at this point, with Eq. (A2) (relation between *K* and α), the lowest critical value of α and root of Eq. (18) is specified. Using the RL method, for pumping between 0 and 1.5 (as constant values), the obtained critical roots (C_{RL}) and their corresponding α are shown in Table I.

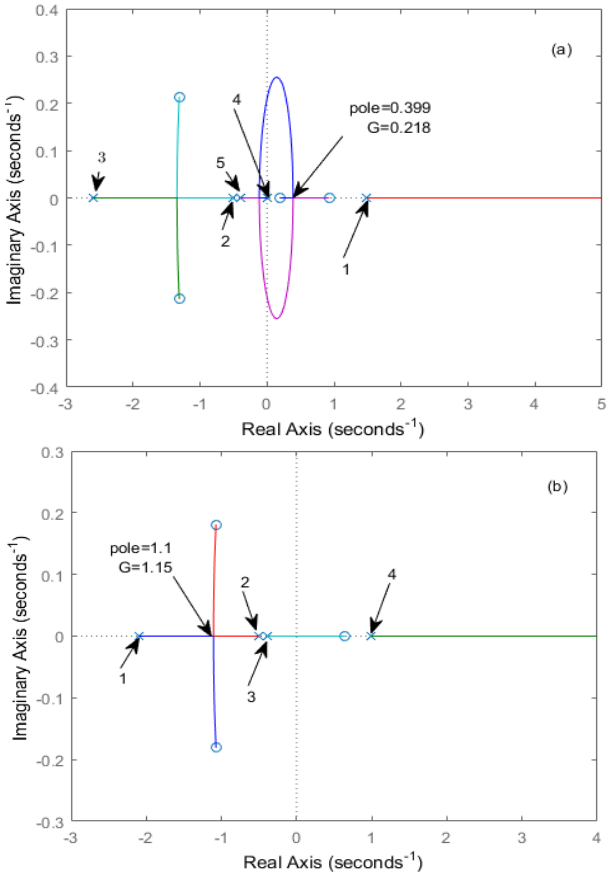

Fig. 2. Root-locus plot of $K=\frac{1}{G}$ (a) for *G*=0:218, (b) for *G*=1:15.

[Downloaded from mail.ijop.ir on 2026-11-26]

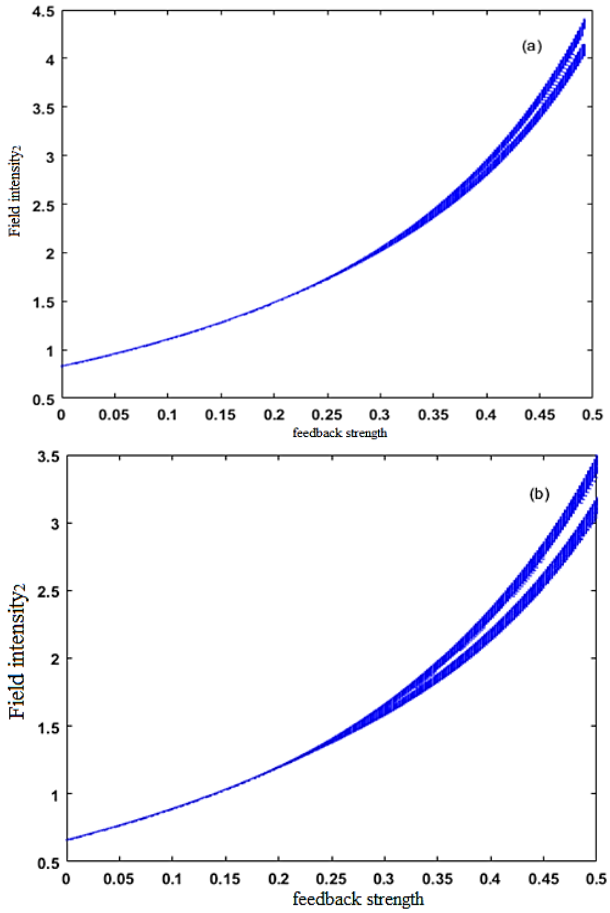

Fig. 3. Bifurcation diagrams corresponding to the domain of electric field $|E|^2$ with η as the bifurcation parameter. The different bifurcation diagrams have been obtained from Eqs. (4)-(8). a) for α=1.1374, and P=0.5 and b) for α=1.29384, and P=0.

Following the strategy of [7], [43], we can estimate the limit of this validity around $\eta = 0.5$. The values of η obtained in this paper are lower than this limit. For example, to indicate the accuracy of the described method in finding the first Hopf point, the values of α=1.2938 and 1.1374 from Table 1 have been selected for numerical solution, drawing branches, and time series graphs. The obtained results are confirmed by bifurcation diagrams (Fig. 3) that show the first Hopf bifurcation and Hopf point. In Figs. 3(a) and 3(b), the output dynamics of the QCL subject to FPCF have been depicted as a function of feedback strengths for α=1.1374, P=0.5 and α=1.2938, P=0.4, respectively. In Figs. 3(a) and 3(b), for some positive values of the η, $|E|^2$ operates in the periodic and stable dynamic. In addition, the decrease of η (at η=0.22 and η =0.256) leads to the appearance of a doubling period and Hopf bifurcation. To confirm the above dynamics, the time series $|E|^2$ have been checked for two bifurcation diagrams. The results are shown in Figs. 3(a) and 3(b) for the Figs. 2(a) and 2(b) respectively. As can be seen, for $|E|^2$ in terms of time (ps), η=0.205 (Fig. 3(a)) and η=0.328 (Fig. 3(b)) are the first Hopf points.

Now, by considering the obtained values (in Table 1), the expression that generates the critical roots of Eq. (18) has been investigated. This relation is obtained by the Particle Swarm Optimization (PSO) algorithm in the next section.

VI. PARTICLE SWARM OPTIMIZATION (PSO) ALGORITHM

In computational science, the PSO algorithm is a computational method for optimizing continuous nonlinear functions that are best presented by explaining its conceptual development and are computationally efficient [33]. PSO, by having a population of particles, solves the problem, which optimizes a problem through repeated action and improves a candidate solution due to the given measure of quality [44]. Due to its many advantages, including its simplicity and easy implementation, the most optimist solution can be worked out in the particle swarm optimization algorithm, and it can be used to work out complex problems.

PSO is used widely in fields such as function optimization, model classification, signal procession, vague system control, etc. [45], [46].

In this paper, a type of the PSO algorithm using a population (obtained roots in Table I) of candidate solutions (particles (C_{PSO})) works. These particles tend to move around the D-dimensional search space [43] (poles versus α and P), the obtained relation according to the:

$$C_{PSO} = A_1\sqrt{P}\left(P^{1/4} - A_2\sqrt{\alpha} + A_3\alpha\right) \qquad (20)$$

[Downloaded from mail.ijop.ir on 2026-11-26]

The particles are moved under their own best position and the best position of the swarm [33]. When the best positions are discovered (based on A_1, A_2, and A_3 coefficients), these are used to guide the movements of the swarm.

The procedure continues until an optimal solution is finally attained. Finally, in Eq. (20), the coefficients A_1, A_2, and A_3 are obtained as A_1=0.56324, A_2=0.005 and A_3=0.1377.

Fig. 4 shows the changes of particle and root in the search space (Three-dimensional trajectory of poles versus α and P). In this figure, the blue dashed line and red line present the obtained roots by the RL method and the particles (obtained roots by PSO (in Table 1)), respectively. Eq. (20) is the best approximation of the expression that generates the nearest values to the C_{RL}. Table 1 presents the roots generated by C_{PSO} and C_{RL}.

Table 1. The achieved and calculated results values for C by PSO Algorithm (C_{PSO}) versus RL method (C_{RL}).

C_{RL}	C_{PSO}	α	P
0	0	0	0
0.1430	0.1159	0.6735i	0.1
0.2280	0.2268	1.7321	0.2
0.2830	0.2895	1.4850	0.3
0.3380	0.3447	1.2938	0.4
0.3990	0.3951	1.1374	0.5
0.4470	0.4421	1.0040	0.6
0.4800	0.4863	0.8864	0.7
0.5530	0.5282	0.7796	0.8
0.5730	0.5684	0.6828	0.9
0.5990	0.6065	0.5866	1.0
0.6360	0.6430	0.4937	1.1
0.6830	0.6772	0.3934	1.2
0.7050	0.7086	0.2785	1.3
0.7500	0.7330	0.1005	1.4
0.7820	0.7825	0.2182i	1.5

Using Eqs. (15) and (18), the following expression for the feedback strength is obtained:

$$\eta = C_{PSO}\sqrt{\left(1+\alpha^2\right)} \tag{21}$$

where C_{PSO} is given by Eq. (20).

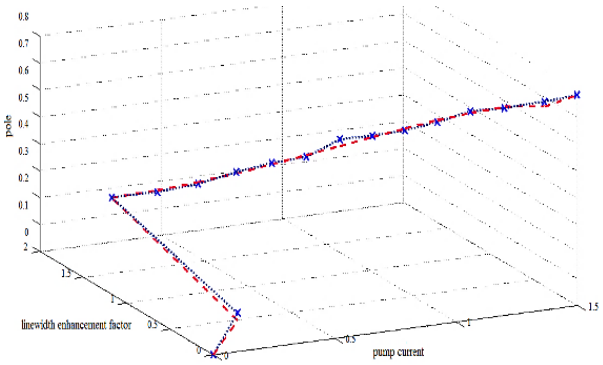

Fig. 4. Particle and Root variations in search space (poles versus α and P).

To study our critical expression outputs for feedback strength, we numerically investigate this equation and the change of the critical values (as first Hopf bifurcation) of η versus α and P as control parameters. Fig. 5 shows the Critical feedback strength η as a function of the LEF α pump parameter P and it can be said that it is corresponds to the stability boundaries for QCL with FPCF. The vertical and horizontal axis represents the feedback strength η and α, respectively. By increasing α, feedback strength values indicate the tendency to decrease. For example, when the linewidth enhancement factor increases above $\alpha > 1.6$, the system becomes destabilized nearly the η=0.45. Figure 5 shows that in the presence of Hopf bifurcation, the system becomes destabilized by values of LEF. It can be seen in the figure, increasing the pump parameter increments the value of the feedback strength η. According to the results of previous studies, decreasing the value of α increases the strength of the feedback and thus increases the stability. For example, in [8], an increase in α led to a reduction in the critical feedback strength. Compared to [8], QCL subject to FPCF with QCL subject to PCF, at α=1.5, the value of feedback strength for PCF is about 0.3, and for FPCF is about 0.5. Therefore, it can be said that the QCL subject to FPCF has more stability than the PCF. Then we intend to compare QCL subject FPCF with COF [7]. For instance, at α=1.5, for COF, the value of η it should be about 0.2 and 0.28 [7], [18]. Therefore, for the realistic amount of the parameters, it can be said that the QCL with FPCF is remarkably more stable than with PCF and COF cases. Furthermore, if the QCL is in the presence of

[Downloaded from mail.ijop.ir on 2026-11-26]

TOF as the tilt angle increases, the feedback strength η weakens, so the QCL is restabilized and operates in continuous wave emission.

In continue, it has been tried to compare the critical equation (Eq. (21)) obtained in the previous sections with the feedback obtained in [7], [8]. The time series $|E|^2$ were obtained without approximation and by directly numerically solving the equations, and then the time series were plotted using Table 1. According to [6], [10], these time series indicate the Hopf points.

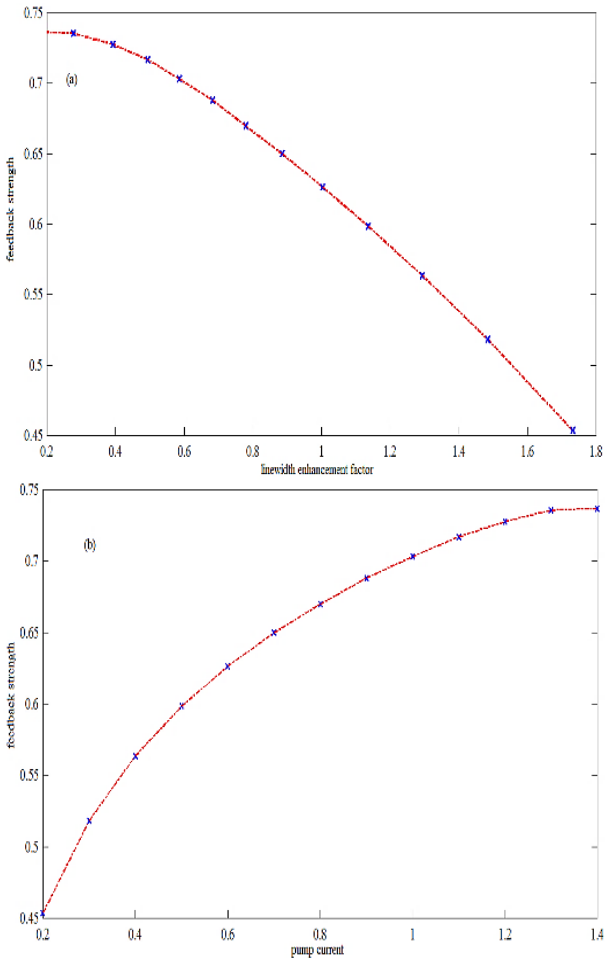

Fig. 5. Critical feedback strength η as a function of the (a) LEF α, (b) for pump parameter P.

VII. CONCLUSION

The objective of this paper is to describe and investigate the properties of quantum cascade lasers under filtered conjugate phase feedback using asymptotic analysis, the RL method, and the PSO algorithm.

Theoretical and experimental studies have demonstrated that optical feedback, depending on feedback strength, can lead to stability and instability dynamics in QCLs [47], [48].

However, it appears that for a more extensive range of feedback strength ratios, a QCL subjected to PCF is more stable than the COF case. The PCF with finite depth tends to suppress chaotic output and produces pulses whose repetition rate is tunable by varying PCF reflectivity [7], [49]. Next, in recent works [2], [10] , it can be said that the QCL is well destabilized by tilted optical feedback, the dynamics of which can be tuned by changing the tilt angle, the instabilities increase as the angle increases [2]. In this study, the FPCF laser showed less instability due to specific values of τ_r , pump current, and small LEF. As a result, for different feedback strength values, the QCL subject to FPCF was found to be more stable when compared to QCL with PCF, COF, and TOF. FPCF is more complex than conventional feedback. It can show better stability performance, especially in the case of distortion. FPCF by adding filtering improves PCF. By incorporating filtering mechanisms, FPCF enhances stability and signal quality [6], [11], [22], [50], [51].

APPENDIX A

To obtain the critical roots of Eq. (16) base of the technique of [39], the equation is rewritten as follows:

$$\begin{aligned} &K(2X+1)^2X^3+B(2X+1)X^2+\\ &+F(2X+1)^2X^2+D(2X+1)X+\\ &+E(2X+1)^2X-Gh+G(2X+1)=0 \end{aligned} \tag{A1}$$

$$\begin{aligned} &K=2\left(1+\alpha^2\right),\ B=-2\left(1+\alpha^2\right)I(\gamma+1)\\ &F=2\left(1+\alpha^2\right)-4\gamma,\\ &D=\gamma I\left((2\gamma+1)-\left(1+\alpha^2\right)\right),\\ &E=-2\gamma,\ G=\gamma^2 I,\ h=I \end{aligned} \tag{A2}$$

[Downloaded from mail.ijop.ir on 2026-11-26]

$$X^5\left[4K+X^4\left(8\left(K-2\gamma\right)\right)\right]+$$
$$X^3\left[5K-2KI\left(\left(\gamma+1\right)-24\gamma\right)\right]+$$
$$X^2\left\{-KI\left(\gamma+1\right)+K-12\gamma+2\gamma I\left[\left(2\gamma+1\right)-\frac{K}{2}\right]\right\}$$
$$X\left\{\gamma I\left[\left(2\gamma+1\right)-\frac{K}{2}\right]-2\gamma+2\gamma^2 I\right\}-\gamma^2 I\left(I-1\right)=0 \quad \text{(A3)}$$

Finally, for clarity and understanding, we simplify the Eq. (A3) as Eq. (19).

APPENDIX B

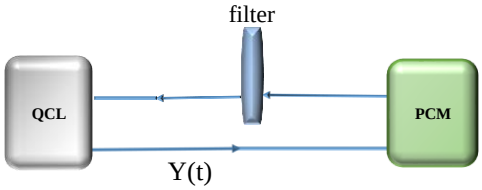

Fig. 6. Schematic diagram of QCL subject to a filtered-phase-conjugated feedback [6], [23].

Figure 6 shows a schematic of the system for a quantum cascade laser under filtered-phase-conjugated feedback. The beam output from the quantum cascade laser encounters a phase-conjugate mirror that corrects any distortion and reflects it to its original path. Next, a filter would be placed in the path, which is selected to allow certain wavelengths of light to pass through.

Assuming that $Y(t)$ is the electric field and, $F(t)$ complex feedback field, for the finite response of a phase-conjugate mirror, the associated equations are written as Eqs. (1)-(3) for such a system. Spectral filtering of the complex feedback field, suppressing frequencies larger than $\frac{1}{\tau_r}$. Therefore, it was seen that with increasing τ_r, the stability increases slightly [6], [23], [52].

Declaration of Competing Interest

The authors declare that they have no known competing financial interests or personal relationships that could have appeared to influence the work reported in this paper.

Funding

This research did not receive any specific grant from funding agencies in the public, commercial, or not-for-profit sectors [47].

REFERENCES

[1] M. Li, Y. Wang, X. Xu, and Y. Tan, "Noise suppression of relaxation oscillation intensity in a microcavity Raman laser," Opt. Laser Technol., vol. 148, pp. 107741, 2022.

[2] X.-G. Wang, B.-B. Zhao, Y. Deng, V. Kovanis, and C. Wang, "Nonlinear dynamics of a quantum cascade laser with tilted optical feedback," Phys. Rev. A., vol. 103, pp. 023528(1-7), 2021.

[3] D.E. Eba, A.D. Mengue, and B.E. Zobo, "Multiscroll chaotic attractors in Optical Injected Semiconductor Laser Driven by a Resonant Tunneling Diode Current," Optik (Stuttg)., vol. 212, pp. 164740(1-8), 2020.

[4] X. Liao. X. Wang, K. Zhou, W. Guan, Z. Li, X. Ma, C. Wang, J.C. Cao, C. Wang, and H. Li, "Terahertz quantum cascade laser frequency combs with optical feedback," Opt. Express, vol. 30, pp. 35937-35950, 2022.

[5] J.Y. Law and G. P. Agrawal, "Effects of optical feedback on static and dynamic characteristics of vertical-cavity surface-emitting lasers," IEEE J. Sel. Top. Quantum Electron., vol. 3, pp. 353–358, 1997.

[6] J. Ohtsubo, *Semiconductor Lasers*, in Springer Series in Optical Sciences, Springer International Publishing., vol. 111, pp. XXV-666, 2017.

[7] G. Friart, G. Van der Sande, G. Verschaffelt, and T. Erneux, "Analytical stability boundaries for quantum cascade lasers subject to optical feedback," Phys. Rev. E, vol. 93, pp. 052201(1-6), 2016.

[8] L. Weicker, D. Wolfersberger, and M. Sciamanna, "Stability analysis of a quantum cascade laser subject to phase-conjugate feedback," Phys. Rev. E, vol. 98, pp. 012214(1-7), 2018.

[9] A. Murakami and J. Ohtsubo, "Dynamics and linear stability analysis in semiconductor lasers with phase-conjugate feedback," IEEE J. Quantum Electron., vol. 34, pp. 1979–1986, 2002.

[Downloaded from mail.ijop.ir on 2026-11-26]

[10] L. Weicker, T. Erneux, D. Wolfersberger, and M. Sciamanna, "Laser diode nonlinear dynamics from a filtered phase-conjugate optical feedback," Phys. Rev. E., vol. 92, pp. 022906(1-7), 2015.

[11] B.-B. Zhao, X.-G. Wang, and C. Wang, "Low-Frequency Oscillations in Quantum Cascade Lasers With Tilted Optical Feedback," IEEE J. Sel. Top. Quantum Electron., vol. 28, pp. 1–7, 2022.

[12] O. Spitz, J. Wu, M. Carras, C.-W. Wong, and F. Grillot, "Chaotic optical power dropouts driven by low frequency bias forcing in a mid-infrared quantum cascade laser," Sci. Rep., vol. 9, no. 1, pp. 4451(1-9), 2019.

[13] J. Liu, Z. Tong, W. Zhang, J. Li, and Y. Li, "Switchable and tunable multi-wavelength erbium-doped random distributed feedback fiber laser based on a compound filter," Optik (Stuttg)., vol. 241, pp. 167015(1-9), 2021.

[14] V. Girardeau, O. Jacquin, O. Hugon, and E. Lacot, "Ultrasound vibration measurements based on laser optical feedback imaging," Appl. Opt., vol. 57, pp. 7634-7643, 2018.

[15] A. Jafari, K. Mabhouti, S. Afrang, and A. Siahcheshm, "Control of instability in a semiconductor laser using a functional pump current generator with a dynamical parameter," Opt. Laser Technol., vol. 44, pp. 1398–1405, 2012.

[16] G. Abbasi and Z. Alaie, "The impact of additional injected signals on the stability and bandwidth of the quantum cascade lasers with external cavities," Optik (Stuttg)., vol. 254, pp. 168653, 2022.

[17] T. Erneux, V. Kovanis, and A. Gavrielides, "Nonlinear dynamics of an injected quantum cascade laser," Phys. Rev. E, vol. 88, pp. 032907(1-8), 2013.

[18] O. Spitz and F. Grillot, "A review of recent results of mid-infrared quantum cascade photonic devices operating under external optical control," J. Phys. Photon., vol. 4, pp. 022001(1-21), 2022.

[19] R. Heinrich, A. Popescu, R. Strzoda, A. Hangauer, and S. Höfling, "High resolution quantitative multi-species hydrocarbon gas sensing with a cw external cavity quantum cascade laser based spectrometer in the 6–11 μ m range," J. Appl. Phys., vol. 125, pp. 134501(1-10), 2019.

[20] F.-Y. Lin and J.-M. Liu, "Chaotic lidar," IEEE J. Sel. Top. Quantum Electron., vol. 10, pp. 991-997, 2004.

[21] O. Spitz, P. Didier, L. Durupt, T. Diaz , A. Daniel, Alexei N, L. Cerutti, and F. Grillot, "Free-Space Communication With Directly Modulated Mid-Infrared Quantum Cascade Devices," IEEE J. Sel. Top. Quantum Electron., vol. 28, pp. 1–9, 2022.

[22] Y.-B. Peng, B.-B. Zhao, and C. Wang, "Nonlinear dynamics of a quantum cascade laser with optical injection," Opt. Express, vol. 30, pp. 27593-27601, 2022.

[23] D. H. DeTienne, G. R. Gray, G. P. Agrawal, and D. Lenstra, "Semiconductor laser dynamics for feedback from a finite-penetration-depth phase-conjugate mirror," IEEE J. Quantum Electron., vol. 33, pp. 838-844, 1997.

[24] D. H. DeTienne, G. R. Gray, G. P. Agrawal, and D. Lenstra, "Semiconductor laser coupled to a finite-response time phase-conjugate mirror," Physics and Simulation of Optoelectronic Devices., vol. 2693, pp. 689-700, 1996.

[25] T. Gensty, W. Elsäßer, and C. Mann, "Intensity noise properties of quantum cascade lasers," Opt. Express, vol. 13, pp. 2032-2039, 2005.

[26] J.R. Dorfman, *An Introduction to Chaos in Nonequilibrium Statistical Mechanics*, Cambridge University Press, vol. 14, pp. 287, 1999.

[27] S. Behnia, S. Afrang, A. Akhshani, and K. Mabhouti, "A novel method for controlling chaos in external cavity semiconductor laser," Opt.-Int. J. Light Electron Opt. (Optik), vol. 124, pp. 757–764, 2013.

[28] H. Chapellat and S. P. Bhattacharyya, "A generalization of Kharitonov's theorem; Robust stability of interval plants," IEEE Trans. Automat. Contr., vol. 34, pp. 306–311, 1989.

[29] Nusret Tan and D. P. Atherton, "Stability and performance analysis in an uncertain world," Comput. Control Eng. J., vol. 11, pp. 91–101, 2000.

[30] A. G. Gad, "Particle Swarm Optimization Algorithm and Its Applications: A Systematic Review," Arch. Comput. Methods Eng., vol. 29, pp. 2531–2561, 2022.

[Downloaded from mail.ijop.ir on 2026-11-26]

[31] A. Gupta and S. Srivastava, "Comparative Analysis of Ant Colony and Particle Swarm Optimization Algorithms for Distance Optimization," Procedia Comput. Sci., vol. 173, pp. 245–253, 2020.

[32] M. C. M. Teixeira, E. Assuncao, and E. R. M. D. Machado, "A Method for Plotting the Complementary Root Locus Using the Root-Locus (Positive Gain) Rules," IEEE Trans. Educ., vol. 47, pp. 405–409, Aug. 2004.

[33] D. Wang, D. Tan, and L. Liu, "Particle swarm optimization algorithm: an overview," Soft Comput., vol. 22, pp. 387–408, Jan. 2018.

[34] L. Jumpertz, *Nonlinear photonics in mid-infrared quantum cascade lasers*, Springer theses, p. XXIII-134, 2017.

[35] J. Faist, *Quantum Cascade Lasers. Oxford* University Press, 2013.

[36] S. Pawłowski and M. Mączka, "Optimisation of QCL Structures Modelling by Polynomial Approximation," Materials, vol. 15, pp. 5715(1-18), 2022.

[37] L. Jumpertz, F. Michel, R. Pawlus, W. Elsässer, K. Schires, M. Carras, and F. Grillot, "Measurements of the linewidth enhancement factor of mid-infrared quantum cascade lasers by different optical feedback techniques," AIP Adv., vol. 6, pp. 015212(1-7), 2016.

[38] T. Erneux, A. Gavrielides, K. Green, and B. Krauskopf, "External cavity modes of semiconductor lasers with phase-conjugate feedback," Phys. Rev. E, vol. 68, pp. 66205(1-9), 2003.

[39] M. C. M. Teixeira, "Direct expressions for Ogata's lead-lag design method using root locus," IEEE Trans. Educ., vol. 37, pp. 63–64, 1994.

[40] M. C. M. Teixeira and E. Assuncao, "On lag controllers: design and implementation," IEEE Trans. Educ., vol. 45, pp. 285–288, 2002.

[41] K. Ogata and J. Brewer "Modern Control Engineering," J. Dyn. Sys., Meas., Control., vol. 93, p. 63, 1971.

[42] L.A. Penny, *Root locus analysis with special partitioning*, Monterey, California. Naval Postgraduate School, Engineering, 1967.

[43] D. Lenstra, G. Vemuri, and M. Yousefi, *Unlocking Dynamical Diversity: Optical Feedback Effects on Semiconductor Lasers*, John Wiley & Sons., pp. 55–80, 2005.

[44] G. Zhang, X. Shao, P. Li, and L. Gao, "An effective hybrid particle swarm optimization algorithm for multi-objective flexible job-shop scheduling problem," Comput. Ind. Eng., vol. 56, pp. 1309–1318, 2009.

[45] Q. Bai, "Analysis of Particle Swarm Optimization Algorithm," Comput. Inf. Sci., vol. 3, pp. 180-184, 2010.

[46] V. Selvi and D. R. Umarani, "Comparative Analysis of Ant Colony and Particle Swarm Optimization Techniques," Int. J. Comput. Appl., vol. 5, pp. 1–6, 2010.

[47] F.P. Mezzapesa, L.L. Columbo, M. Brambilla, M. Dabbicco, S. Borri, M.S. Vitiello, H. E. Beere, D.A. Ritchie, and G. Scamarcio, "Intrinsic stability of quantum cascade lasers against optical feedback," Opt. Express., vol. 21, pp. 13748-13757, 2013.

[48] O. Spitz, J. Wu, A. Herdt, M. Carras, W. Elsaber, C-W. Wong, and F. Grillot, "Investigation of Chaotic and Spiking Dynamics in Mid-Infrared Quantum Cascade Lasers Operating Continuous-Waves and Under Current Modulation," IEEE J. Sel. Top. Quantum Electron., vol. 25, pp. 1–11, 2019.

[49] M. C. Simon Ferré, L. Jumpertz, Kevin Schires, M. Carras, and F. Grillot "Nonlinear dynamics of quantum cascade lasers with optical feedback," Conf. SPIE OPTO., 2015.

[50] Z. Abdul Sattar and K. A. Shore, "Phase Conjugate Feedback Effects in Nano-Lasers," IEEE J. Quantum Electron., vol. 52, pp. 1–8, 2016.

[51] G. Bouchez, T. Malica, D. Wolfersberger, and M. Sciamanna, "Manipulating the chaos bandwidth of a semiconductor laser subjected to phase-conjugate feedback," in Semiconductor Lasers and Laser Dynamics IX., vol. 11356, pp. 106-113, 2020.

[52] W. A. van der Graaf, L. Pesquera, and D. Lenstra, "Stability of a diode laser with phase-conjugate feedback," Opt. Lett., vol. 23, pp. 256-258, 1998.

[Downloaded from mail.ijop.ir on 2026-11-26]



Fahimeh Bakhsheshi is a PhD student in Optical and Laser Physics, Department of Physics, Urmia University, Urmia, Iran. Her research interests include semiconductor lasers.



Khosro Mabhouti is an associate professor of physics in the Department of Physics, Urmia University, Urmia, Iran. Linear and nonlinear optics and laser dynamics are some of his research areas.



Rahim Naderali is an associate professor of physics in the Department of Physics, Urmia University, Urmia, Iran. Quantum optics and laser dynamics are some of his research areas.



Ali Mahmoudlou is an assistant professor in the Department of Physics, Farhangian University, Tehran, Iran.

[Downloaded from mail.ijop.ir on 2026-11-26]